The Astrophysical Journal, 964:14 (9pp), 2024 March 20 https://doi.org/10.3847/1538-4357/ad284c

Intermittency and Dissipative Structures Arising from Relativistic Magnetized Turbulence

Zachary Davis[1], Luca Comisso[2], and Dimitrios Giannios[1]
[1] Department of Physics, Purdue University, 525 Northwestern Avenue, West Lafayette, IN 47907, USA; zkd@purdue.edu
[2] Department of Astronomy and Columbia Astrophysics Laboratory, Columbia University, New York, NY 10027, USA
Received 2023 November 20; revised 2024 January 30; accepted 2024 February 10; published 2024 March 12

Abstract

Kinetic simulations of relativistic turbulence have significantly advanced our understanding of turbulent particle acceleration. Recent progress has highlighted the need for an updated acceleration theory that can account for particle acceleration within the plasma's coherent structures. Here, we investigate how intermittency modeling connects statistical fluctuations in turbulence to regions of high-energy dissipation. This connection is established by employing a generalized She–Leveque model to characterize the exponents ζ_p for the structure functions $S^p \propto l^{\zeta_p}$. The fitting of the scaling exponents provides us with a measure of the codimension of the dissipative structures, for which we subsequently determine the filling fraction. We perform our analysis for a range of magnetizations σ and relative fluctuation amplitudes $\delta B_0/B_0$. We find that increasing values of σ and $\delta B_0/B_0$ allow the turbulent cascade to break sheetlike structures into smaller regions of dissipation that resemble chains of flux ropes. However, as their dissipation measure increases, the dissipative regions become less volume filling. With this work, we aim to inform future turbulent acceleration theories that incorporate particle energization from interactions with coherent structures within relativistic turbulence.

Unified Astronomy Thesaurus concepts: Plasma astrophysics (1261); High energy astrophysics (739); Magnetic fields (994); Relativistic jets (1390)

1. Introduction

A central goal in high-energy astrophysics is to uncover the physical processes that power the most extreme particle accelerators, which are accountable for bright electromagnetic observations. Often, as is the case with gamma-ray bursts and jets from active galactic nuclei, the sources are observed to have a broad electromagnetic spectrum, whose interpretation requires a relativistic nonthermal distribution of particles undergoing radiative cooling (Band et al. 1993; Ghisellini et al. 1998). The mechanisms responsible for the rapid particle acceleration needed to produce these nonthermal particle distributions are a subject of ongoing debate (see Matthews et al. 2020 for a recent review). Nonetheless, it is commonly assumed that the free energy required for particle acceleration comes from large-scale perturbations within the jet, which can lead to the formation of shocks (e.g., Böttcher & Dermer 2010) or large-scale magnetic reconnection layers (e.g., Giannios 2013). Regardless of the specific scenario, a large-scale separation exists from the energy injection scale to plasma kinetic scales, where energy dissipation occurs. This scale separation typically involves turbulence modulation, highlighting the need to understand turbulence for a comprehensive understanding of particle acceleration and high-energy emission.

Turbulence, a complex nonlinear phenomenon already challenging the study of hydrodynamical fluids on Earth, poses additional challenges in astrophysical plasmas. Factors such as low particle collisionality, strong magnetic fields, relativistic velocities, and extreme temperatures contribute to the complexity. The analytical treatment of turbulence often relies on phenomenological cascade models (or scaling theories) that link large-scale fluid fluctuations to smaller scales, extending down to the dissipation scale. The most renowned model of hydrodynamic turbulence is due to Kolmogorov (1941), with adaptations later developed for magnetohydrodynamics (MHD; e.g., Iroshnikov 1963; Kraichnan 1965; Goldreich & Sridhar 1995). Initial investigations into the validity of cascade models were conducted through numerical simulations using the MHD approximation. However, recent progress in this field has seen the development of first-principle kinetic simulations, which are crucial for enhancing our understanding of turbulence in weakly collisional plasmas, particularly at the smallest scales where most energy is dissipated.

Given its relevance in relativistic magnetized outflows, we focus on investigating turbulence in conditions where the magnetic energy density exceeds the rest-mass energy density and the plasma pressure. Under these conditions, plasma motions approach the speed of light, marking the *relativistic turbulence* regime. This regime of turbulence is intrinsically linked to magnetic reconnection (Lazarian et al. 2012; Comisso & Sironi 2019), which has been shown to be an efficient accelerator of relativistic particles (e.g., Comisso & Sironi 2018). Additionally, in the relativistic regime, the stochastic Fermi acceleration mechanism (Fermi 1949) operates on short timescales, facilitating the rapid conversion of magnetic energy into plasma particle energy. Turbulent acceleration in magnetized plasmas has been associated with various sources of high-energy emissions, including solar flares (Miller et al. 1996), gamma-ray bursts (Bykov & Meszaros 1996), and blazar jets (Marscher 2014; Davis et al. 2022; Zhang et al. 2023).

The traditional analytical approach to understanding turbulence's role in particle acceleration is through quasi-linear theory (QLT; Bernstein & Engelmann 1966). In QLT, particle trajectories are gyroaveraged before scattering off plasma waves,

and the analytical description often involves calculating a diffusion tensor derived from linear eigenmodes of the plasma's MHD waves (see, e.g., Demidem et al. 2020). However, large-amplitude turbulent fluctuations invalidate QLT, and recent fully kinetic particle-in-cell (PIC) simulations have indeed cast doubts on the QLT description. In the relativistic turbulence regime, QLT is unable to account for the observed development of pitch-angle anisotropy (Comisso et al. 2020; Comisso & Sironi 2021), recreate the observed particle distributions without unexplained advection coefficients (Zhdankin et al. 2020), or provide a mechanism for the observed acceleration at current sheets (Comisso & Sironi 2019). QLT's inability to describe recent results from PIC simulations has spurred the search for new analytical descriptions of particle acceleration in relativistic turbulence. Lemoine (2021) suggested abandoning the idea that particle acceleration in relativistic turbulence is due to wave interactions and rather that acceleration may be mainly due to a collection of interactions with discrete structures within turbulence. Current sheets are of particular interest because of their common occurrence in magnetized turbulence (Comisso & Sironi 2019; Zhdankin et al. 2020) and, when these sheets undergo reconnection, they efficiently dissipate magnetic energy. Current sheets also provide a link to phenomenological cascade models incorporating dissipative structures (Dubrulle 1994; She & Leveque 1994; Biskamp & Müller 2000) that can be associated with the observed intermittency, pitch-angle anisotropy, and energy spectra (Comisso & Sironi 2019; Zhdankin et al. 2020).

To bridge the gap between phenomenological theories of intermittency and the dissipative structures responsible for particle energization, we analyze PIC simulations of relativistic magnetized turbulence. Our investigation begins with the characterization of the turbulence intermittency and its dependence on two key physical parameters: the plasma magnetization and the amplitude of the magnetic fluctuations with respect to the mean magnetic field. We employ a general log-Poisson model of turbulence to establish a link between the coherent structures and the phenomenological model. Once established, we investigate the filling fractions of these coherent structures. This approach is repeated for different values of plasma magnetization and the level of the magnetic fluctuations to analyze the dependence of the dissipative structure properties on these key plasma parameters. Finally, we discuss the implications for current particle acceleration theories before concluding.

2. Numerical Setup

To investigate the statistics of relativistic magnetized turbulence from a first-principles standpoint, we solve the Vlasov–Maxwell system of equations through the PIC method (Birdsall & Langdon 1985) using the publicly available code TRISTAN-MP (Buneman 1993; Spitkovsky 2005). We perform the numerical simulations in a triply periodic cubic domain L^3 that is discretized into a regular lattice of 1024^3 cells. We initialize a uniform electron–positron plasma with a total particle density of n_0 according to a Maxwell–Jüttner distribution with dimensionless temperature $\theta_0 = k_{\rm B}T_0/mc^2 = 0.3$. Here, T_0 is the initial plasma temperature, $k_{\rm B}$ indicates the Boltzmann constant, m is the electron mass, and c is the speed of light in a vacuum. Turbulence is seeded by initializing a spectrum of magnetic fluctuations having polarizations transverse to a uniform mean magnetic field $\langle \boldsymbol{B} \rangle = B_0 \hat{z}$ (see Comisso & Sironi 2018, 2019 for details). The initial magnetic energy spectrum peaks near $k_p = 6\pi/L$, which defines the energy-carrying scale $l_0 = 2\pi/k_p$ and limits the particles' maximum Lorentz factor through stochastic acceleration (Comisso & Sironi 2018).

The strength of initial fluctuating magnetic energy relative to plasma enthalpy is quantified by

$$\sigma = \frac{\delta B_0^2}{4\pi n_0 w_0 mc^2}, \tag{1}$$

where $\delta B_0 = \langle \delta B^2(t=0) \rangle^{1/2}$ is the initial rms amplitude of the magnetic field fluctuations and $w_0 = [K_3(1/\theta_0)/K_2(1/\theta_0)]$ is the initial enthalpy per particle, with $K_n(z)$ indicating the modified Bessel function of the second kind of order n. The corresponding total magnetization is $\sigma + \sigma_{B_0} = (\delta B_0^2 + B_0^2)/4\pi n_0 w_0 mc^2$. Since our work focuses on studying *relativistic* plasma turbulence, characterized by Alfvénic velocity fluctuations $v_A = c\sqrt{\sigma/(1+\sigma)} \sim c$, we focus on the magnetization regime $\sigma \gg 1$. Our simulations cover a range of magnetizations with values $\sigma \in \{2.5, 5, 10, 20, 40\}$, and different strengths of the mean magnetic field, corresponding to ratios $\delta B_0/B_0 \in \{0.5, 1, 2\}$.

We adopt a spatial resolution of $\Delta x = d_{e0}/3$, implying $L = 1024 d_{e0}/3$, where $d_{e0} = c/\omega_{p0}$ indicates the initial plasma skin depth and $\omega_{p0} = \sqrt{4\pi n_0 e^2/\gamma_{\rm th0} m}$ is the relativistic plasma frequency, where $\gamma_{\rm th0} = w_0 - \theta_0$ is the initial mean thermal Lorentz factor. We employ an average of four computational particles per cell. Earlier studies (Comisso & Sironi 2018, 2019) have demonstrated convergence with respect to these numerical parameters. Since we are interested in studying fully developed turbulence, we ran the simulation up to $t \sim 3l_0/c$, at which point the turbulence has been fully developed. In the following, we mainly discuss the results obtained from the magnetic field $b = B/B_0$, the current density $j = J/en_0c$, and the fluid bulk velocity $v = V/c$, obtained by averaging the velocities of individual particles.

3. Intermittency Model

Turbulence is characterized by a broad range of scales linking energy initially injected at large scale l_0 down to a much smaller scale $l_d \ll l_0$ where energy can be efficiently dissipated. To this day, there is no fully developed theory that comprehensively explains this process. Rather, the best results in explaining the energy cascade have come from building a collection of hypotheses that are then integrated into a phenomenological model.

One of the most celebrated models is Kolmogorov's (referred to as K41; Kolmogorov 1941), which established the phenomenological energy spectrum $E(k) \propto k^{-5/3}$ and introduced the pivotal "4/5 law." This law gives the third moment of velocity fluctuations as $\langle (\delta v(l))^3 \rangle = -\frac{4}{5}\epsilon l$, where ϵ is the cascading energy flux, l is a given eddy size, and

$$\delta v(l) \equiv v(\boldsymbol{r} + \boldsymbol{l}) - v(\boldsymbol{r}) \tag{2}$$

is the velocity fluctuation. Kolmogorov suggested introducing a simple self-similarity assumption to extend this law to a higher power of p. In this case, one has

$$S^p(l) = \langle (\delta v(l))^p \rangle \propto l^{\zeta_p}, \tag{3}$$

with $\zeta_p^{K41} = p/3$ for K41. Though initially successful for hydrodynamical turbulence, deviations from the scaling relation become evident for $p > 3$.

General deviations in ζ_p from $p/3$ are often attributed to intermittency, or the tendency for subsequent eddys to become less volume filling than the previous generation. She & Leveque (1994) proposed a phenomenological model to account for the observed deviations in hydrodynamical turbulence by introducing a recursion relation that resulted in a hierarchy of dissipative structures. From this hierarchy, She & Leveque (1994) derived the relation

$$\zeta_p = (p/g)(1 - x) + C_0[1 - (1 - x/C_0)^{p/g}] \quad (4)$$

for the scaling exponents. Here, Equation (4) is presented as it is in Politano & Pouquet (1995), where the physical assumptions resulting in no free parameters have been removed. In Equation (4), g corresponds to fluctuation scaling (i.e., for velocity, $\delta v_l \propto l^{1/g}$), x relates to cascade timescale of the dissipative structures, $\tau_l \propto l^x$, and C_0 is the codimension of the structures, related to the fractal dimension by $C_0 = d - D$. Here d is the embedded space dimension (i.e., $d = 2$ for 2D turbulence and $d = 3$ for 3D turbulence) and D is the fractal dimension of the structures.

In Dubrulle (1994), it was shown that the model presented in She & Leveque (1994) corresponds to the dissipative structures processing a distribution described by a log-Poisson equation and in the correct limits can be described with a random fractal β model. In the general form presented in Equation (4), we are able to compare different phenomenological models of turbulence. A K41 scaling can be recovered with $x = 0$, $g = 3$, and $C_0 = 0$. To reproduce the exact result in She & Leveque (1994), let $x = 2/3$, $g = 3$, and since She & Leveque (1994) considered filamentary structures, $C_0 = 2$.

Including magnetic fields also has expected effects on the parameters in Equation (4). Following Iroshnikov (1963) and Kraichnan (1965), we can expect $g = 4$ due to a larger cascade time from the Alfvén wave interactions. Goldreich & Sridhar (1995) introduced anisotropy of the magnetic field fluctuations into the picture. This finds $g = 3$ for fluctuations perpendicular to the background magnetic field and $C_0 = 1$ by assuming that dissipation occurs in sheets. Müller & Biskamp (2000) proposed to modify the She & Leveque (1994) model by simply setting $C_0 = 1$ for magnetized turbulence, as turbulent MHD simulations were abundant in electric current sheets.

Instead of presuming the structure of the turbulent fluctuations, in the following, we analyze the simulations discussed in Section 2 using structure function statistics as a tool to characterize intermittency, examine the applicability of previous phenomenological models, and understand how these models relate to the most dissipative structures in turbulence.

4. Structure's Codimensionality

In order to carry out an analysis that can then be compared to phenomenological models, we first outline the construction of the structure function (SF). For simplicity, the analysis is carried out using the magnitude of fluctuation, as seen for the fluid velocity in Equation (2). Due to observed anisotropy in the turbulent spectrum (Müller et al. 2003; Zrake & MacFadyen 2013), we also analyze the parallel component of a fluctuation by letting $\boldsymbol{l}$ go to $\boldsymbol{l}_\parallel$, referring to the fluctuation component parallel to the mean magnetic field, namely $\boldsymbol{B_0}$:

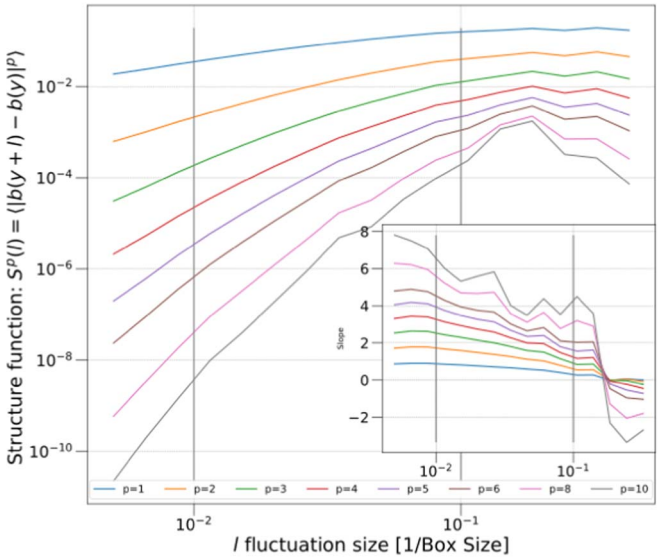

Figure 1. SF of fluctuations in b for p in the range 1–10. Colors denote different values of p. The black vertical lines denote the scales $L = 1/100$ and $L = 1/10$ as fractions of the simulation box size, where the SF is fitted to the power law $\propto l^{\zeta_p}$. The inset shows the slope of the SF.

$$\delta v(l)_\parallel \equiv [\boldsymbol{v}(\boldsymbol{r} + \boldsymbol{l}) - \boldsymbol{v}(\boldsymbol{r})] \cdot \frac{\boldsymbol{l}}{l}. \quad (5)$$

To calculate the value of a given fluctuation for increment l, the simulation grid is split up into 2D slices of thickness l along the given $\boldsymbol{r}$ value. If a slice does not fall on a grid point, the values are linearly interpolated. The slice is then subtracted from another slice separated by the distance l. We repeat this for 150 unique, randomly selected pairs of slices. In order to build an SF with this fluctuation, all subtracted pairs have the absolute value taken, raised to the p before averaging. An example of the produced SF is shown in Figure 1.

To compare and fit to phenomenological models, we calculate the SF exponent ζ_p by fitting the SF to a power law l^{ζ_p}. The fitting range is set from $1/100$ to $1/10$ of the box size to ensure we are consistently within the inertial range. This range is shown in Figure 1. We use a least-squares method for the fit, and the coefficient's error is determined from the covariance matrix. We calculate ζ_p values for orders $p = 1,...,10$ and for quantities δb, δj, and δv. All measurements are then repeated for each simulation. Additionally, we fit Equation (4) for C_0 using again a least-squares fit. Parameters $x = 2/3$ and $g = 3$ are assumed constant. These results are detailed in Table 1.

For illustrative purposes, we show in Figure 2 the general appearance of the scaling exponents for the magnetic field both from the perpendicular and parallel SF. The pronounced intermittency is evident through the large deviation from the K41 scaling after $p = 3$. The red dotted line shows the results from She & Leveque (1994), and we can see that we generally have a significant deviation demanding lower values for the codimension C_0 than those typically found in hydrodynamic turbulence. The parallel direction displays smaller deviations that are closer to the original She & Leveque (1994) value. The smaller deviation in the parallel direction is consistent with what is seen in Zrake & MacFadyen (2013).

Table 1
A Summary Table of the Intermittency Results

	C_0	$C_{0,\parallel}$	σ	$\delta B_0/B_0$
δb	0.963 ± 0.06	1.14 ± 0.08	2.5	1
δb	1.0 ± 0.08	1.3 ± 0.08	5	1
δb	1.09 ± 0.04	1.11 ± 0.03	10	0.5
δb	1.21 ± 0.06	1.76 ± 0.05	10	1
δb	1.23 ± 0.08	2.98 ± 0.02	10	2
δb	1.51 ± 0.04	1.94 ± 0.09	20	1
δb	1.58 ± 0.09	2.2 ± 0.1	40	1
δj	0.7 ± 0.06	0.683 ± 0.06	2.5	1
δj	0.753 ± 0.05	0.685 ± 0.06	5	1
δj	0.718 ± 0.01	0.68 ± 0.03	10	0.5
δj	0.805 ± 0.05	0.701 ± 0.06	10	1
δj	0.796 ± 0.03	0.694 ± 0.03	10	2
δj	0.824 ± 0.08	0.711 ± 0.06	20	1
δj	0.954 ± 0.05	0.728 ± 0.07	40	1
δv	1.08 ± 0.02	2.28 ± 0.01	2.5	1
δv	1.187 ± 0.008	1.98 ± 0.06	5	1
δv	1.03 ± 0.02	1.59 ± 0.02	10	0.5
δv	1.16 ± 0.01	2.05 ± 0.05	10	1
δv	0.817 ± 0.02	2.19 ± 0.04	10	2
δv	0.997 ± 0.02	1.59 ± 0.06	20	1
δv	0.865 ± 0.03	1.69 ± 0.04	40	1

Note. For each variable (δb, δj, and δv), the codimensions C_0 and $C_{0,\parallel}$ are found by fitting Equation (4) for values of $\sigma = 2.5$, 5, 10, 20, and 40 and $\delta B_0/B_0 = 0.5$, 1, and 2.

Figures 3 and 4 illustrate the behavior of the codimensions C_0 and $C_{0,\parallel}$ (for δv, δb, and δj) with respect to the magnetization σ and the turbulence level $\delta B_0/B_0$. C_0 and $C_{0,\parallel}$ exhibit similar trends, albeit slightly higher values for the parallel component. Figures 3 and 4 suggest an almost inverse trend in the fluctuations of velocity (δv) compared to the magnetic field (δb), deviating from the expected scaling in incompressible MHD. This divergence might be attributed to the significant density fluctuations observed in relativistic turbulence. Future investigations could explore whether considering density-weighted fluctuations in velocity, as conducted in Zrake & MacFadyen (2012), could reinstate the incompressible MHD behavior.

As the dissipation of the velocity fluctuations go from filamentary to sheetlike with increasing σ, the magnetic fluctuations go from being dissipated in sheetlike structures to filamentary ones. This suggests that in increasingly magnetized plasmas, more energy is dissipated within flux ropelike structures, as seen in Dong et al. (2022). The general dependence on $\delta B_0/B_0$ is strong for the magnetic field and has a similar trend as is seen in Müller et al. (2003).

5. Dissipative Structures

In collisionless plasmas, a comprehensive theory explaining how the cascade eventually leads to dissipation in this regime is still lacking. Given that energy dissipation must occur through electromagnetic interactions, and that energy is initially stored in the magnetic field, we choose to use the magnetic field cascade to define the codimension C_0 for the dissipative structures. We identify structures with the corresponding C_0 by finding regions characterized by large electromagnetic dissipation. To this purpose, we employ the dissipation measure

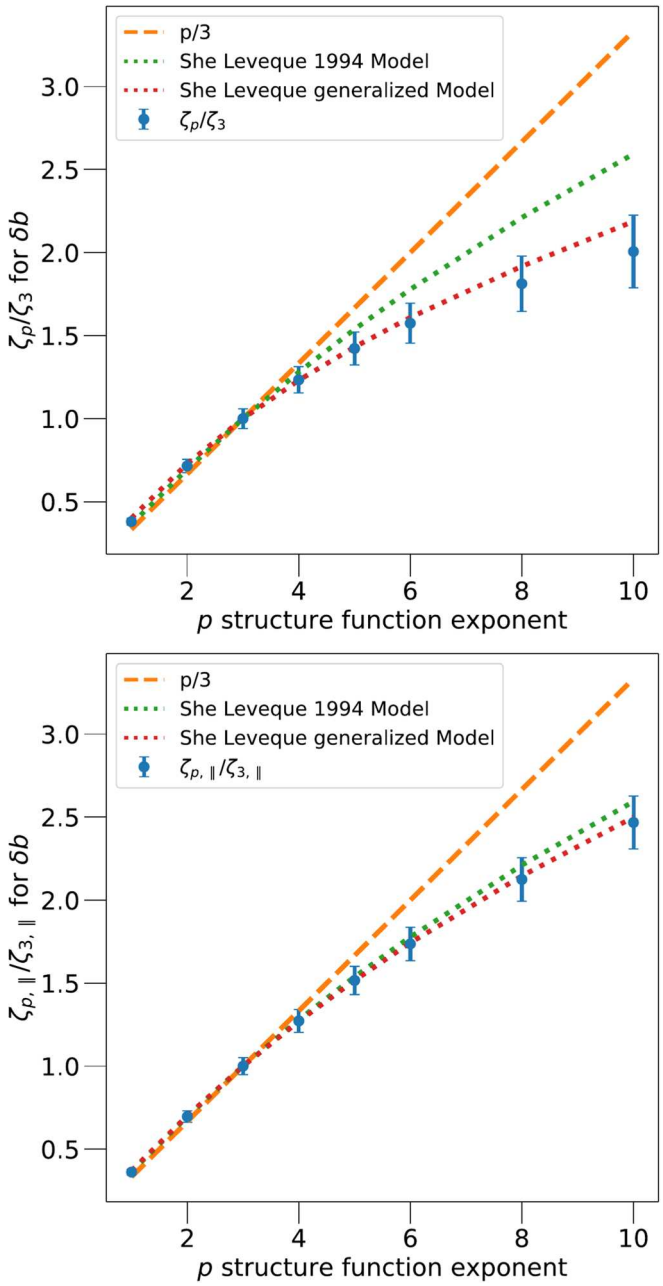

Figure 2. SF exponents ζ_p vs. p for $\sigma = 10$ and $\delta B_0/B_0 = 1$. Compared with the trends from Kolmogorov (1941; orange dashed line) and the result from She & Leveque (1994; green dotted line). The red dotted line shows our fit to data using Equation (4) with $x = 2/3$ and $g = 3$. $C_0 = 1.14$ for the top figure and $C_0 = 1.73$ for the bottom figure.

(Zenitani et al. 2011)

$$D_e = \boldsymbol{J} \cdot (\boldsymbol{E} + \boldsymbol{v}_e \times \boldsymbol{B}) - \rho_e(\boldsymbol{v}_e \cdot \boldsymbol{E}), \tag{6}$$

similarly to Wan et al. (2016) in the context of nonrelativistic turbulence. Equation (6) describes the work done by electromagnetic fields on the particles, evaluated in a frame moving with the electron fluid velocity $\boldsymbol{v}_e$. Here, ρ_e is the charge density and $\boldsymbol{E}$ is the electric field. In order to find the value of the codimension C_0 for structures in D_e, we first establish the fractal dimension for structures defined by $D_e/D_{e,\mathrm{rms}} \geqslant \mathrm{rms}_{\mathrm{cut}}$ using a box-counting algorithm. We plot this for various values of $\mathrm{rms}_{\mathrm{cut}}$ in Figure 5.

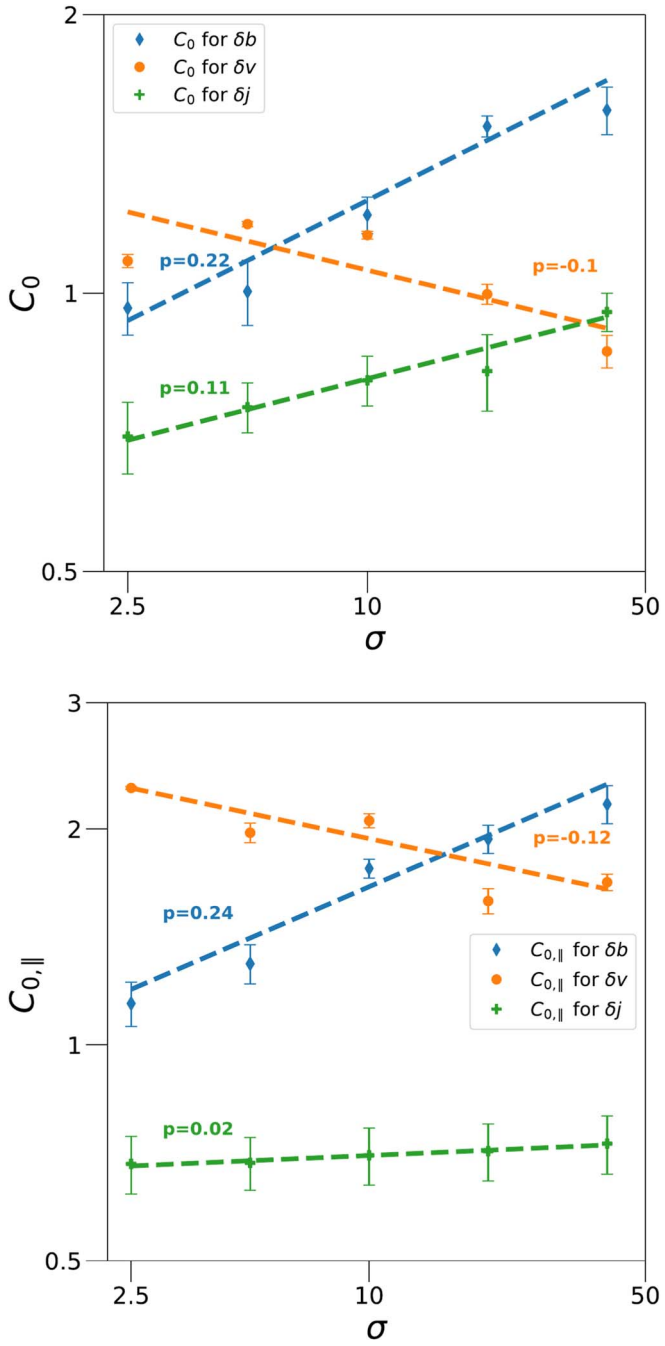

Figure 3. Dependence of the codimensions C_0 and $C_{0,\parallel}$ on σ. Orange, blue, and green denote fluctuations in δv, δb, and δj, respectively. Dashed lines show a power law with a similar slope to data of the corresponding color. The top and bottom figures are in log–log space.

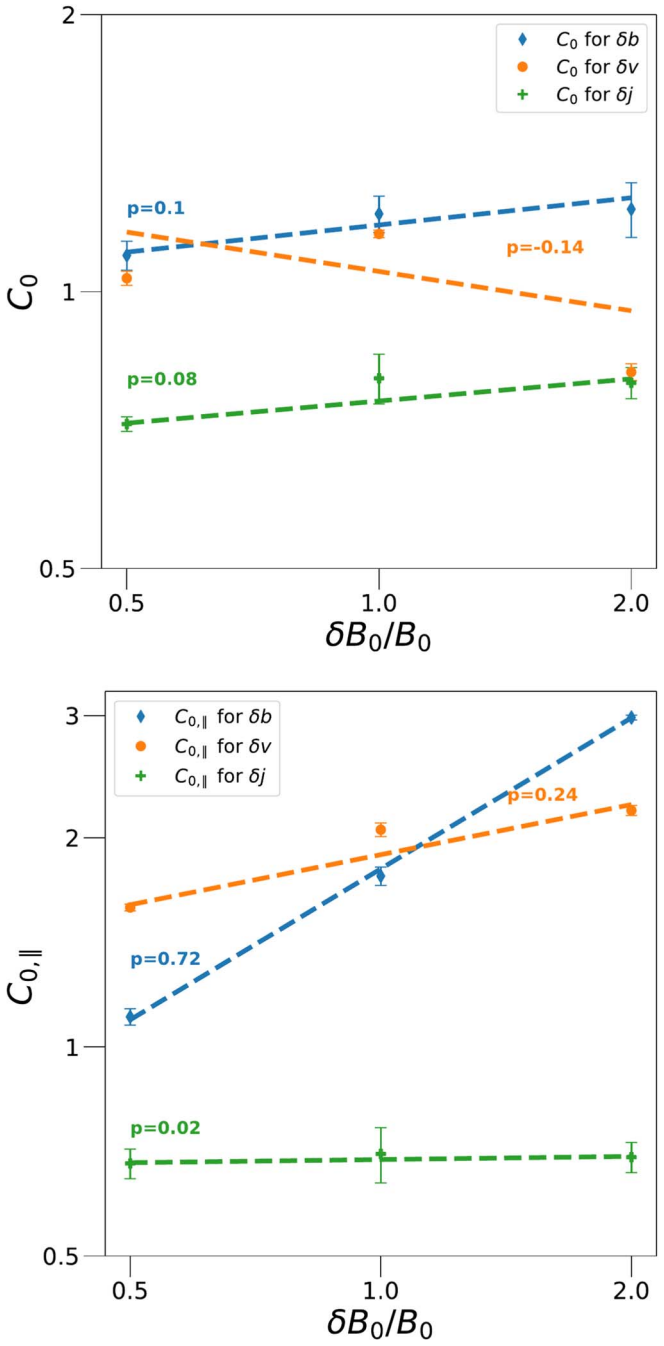

Figure 4. Dependence of the codimensions C_0 and $C_{0,\parallel}$ on $\delta B_0/B_0$. Orange, blue, and green denote fluctuations in δv, δb, and δj, respectively. Dashed lines show a power law with a similar slope to data of the corresponding color. The top and bottom figures are in log–log space.

From this plot, we observe minimal dependence on σ or $\delta B_0/B_0$. Figure 5 enables us to visually identify the values of $\mathrm{rms}_{\mathrm{cut}}$ corresponding to a given codimension C_0, determined earlier by analyzing the SF. In Figure 6 we show a random 2D slice at a given z-coordinate. Structures are highlighted to show regions with a similar value of C_0 in D_e as was found from fitting the SF exponent for δb. The 3D rendering of these structures is shown in the right column of Figure 6.

At low $\sigma = 2.5$, we find a codimension $C_0 \approx 1$, indicative of predominantly sheetlike structures in the dissipation measure D_e. These can be seen in Figure 6 (left) where discrete sheets of dissipation are discernible. In its corresponding 3D figure, we can see that these sheets fill a large part of the volume in comparison to other figures. At $\sigma = 10$, the corresponding $C_0 \approx 1.1$ is highlighted in the D_e structures with an $\mathrm{rms}_{\mathrm{cut}} \approx 3$. Though generally still sheetlike, the volume occupied by these structures is significantly reduced. For $\sigma = 40$, the codimension C_0 increases to ≈ 1.6, but this requires a much higher $\mathrm{rms}_{\mathrm{cut}} \approx 6$. This drastically decreases the occupied volume with small slightly elongated dissipation areas that resemble flux ropes. It is clear that as σ increases, the energy is dissipated in smaller, less volume-filling structures.

To quantify this result, for every simulation in Table 1, we used a bisection algorithm to determine the $\mathrm{rms}_{\mathrm{cut}}$ value that

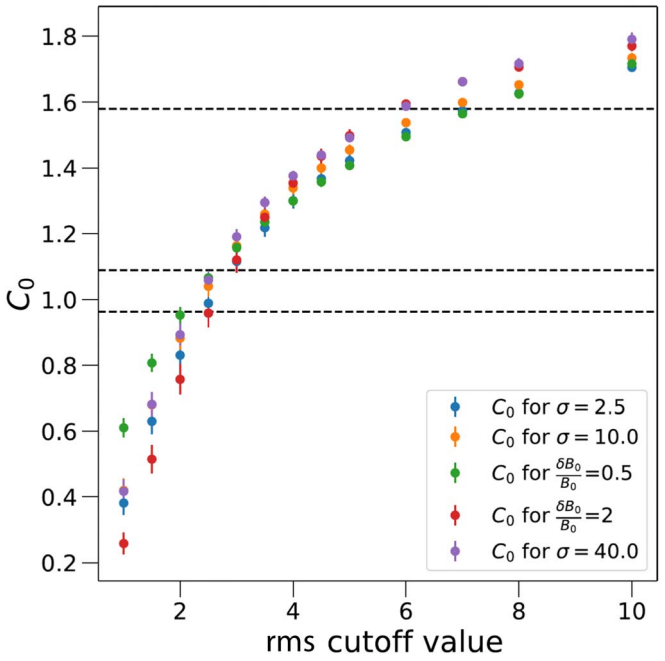

Figure 5. Codimension C_0 for $D_e \geqslant D_{e,\mathrm{rms}} \times \mathrm{rms}_{\mathrm{cut}}$ vs. $\mathrm{rms}_{\mathrm{cut}}$. Horizontal dashed lines indicate C_0 values corresponding to $\sigma = 2.5$, 10, and 40 as listed in Table 1.

identifies structures defined by $|D_e| \geqslant |D_{e,\mathrm{rms}}| \times \mathrm{rms}_{\mathrm{cut}}$ with the same value for C_0 as listed in Table 1 within an error margin of $\pm 1\%$. Then, $f = N_{D_e}/N$ represents the filling fraction or the number of cells where $|D_e| \geqslant |D_{e,\mathrm{rms}}| \times \mathrm{rms}_{\mathrm{cut}}$. Additionally, we define $q_f = f_+/f_-$, where f_+ is the filling fraction for structures defined by $D_e \geqslant D_{e,\mathrm{rms}} \times \mathrm{rms}_{\mathrm{cut}}$, and f_- is the filling fraction for structures defined by $D_e \leqslant -|D_{e,\mathrm{rms}}| \times \mathrm{rms}_{\mathrm{cut}}$. The error bars for both f and q_f are derived from repeating these calculations using the upper and lower bounds of the original C_0 as reported in Table 1.

Results for f can be seen in Figure 7 to be generally trending to smaller values before appearing to approach a constant as σ increases. Larger values of $\delta B_0/B_0$ also result in a decreased filling fraction of the inferred structures (Figure 7). The ratio q_f appears in Figure 8 to increase rapidly with σ before it potentially plateaus. Additional data simulations will be required to determine if the trend continues for larger values of σ. The impact of $\delta B_0/B_0$ on q_f is shown in the bottom frame of the same figure, revealing a steep decreasing trend.

6. Discussion and Conclusions

When examining the identified dissipative structures, a trend emerges, showcasing a preference for more compact regions of dissipation (Figure 6) as the magnetization σ increases. This tendency may be attributed, in part, to current sheets becoming increasingly tearing unstable for larger values of σ (and $\delta B_0/B_0$), resulting in the disruption of current sheets with a broader thickness λ_d. The disruption of these sheets enables the cascade to extend into smaller regions where the dissipation measure becomes stronger. In Comisso & Sironi (2019), λ_d is derived and shown to have a strong dependence on the plasma's enthalpy. Higher values of σ increase the available free energy, leading to enhanced plasma heating and consequently an increase in λ_d. In future work, we aim to explore the potential link between the most dissipative structures and the formation of flux ropes via tearing instability.

In Comisso & Sironi (2018, 2019) it was shown that turbulent acceleration is a two-stage process with the first being initial rapid acceleration associated with current sheets, and the second being a stochastic Fermi-like process. The initial rapid acceleration works as an injection process for the particles and is controlled by the parallel electric field, thereby establishing a preferred direction of motion along the magnetic field for particles around this injection energy. If these same features investigated here predominantly operate through the parallel electric field, then understanding the distribution of these structures may provide a link to understanding the anisotropic features that arise in relativistic turbulence. Specifically, combining the distribution of coherent structures with the rate of plasma processed by a reconnecting current sheet, given by the reconnection rate $\beta_R = v_R/c \approx 0.1\delta B_0/\sqrt{\delta B_0^2 + B_0^2}$ (Comisso & Jiang 2023), we can approximate the average power per unit area experienced by the plasma from the parallel electric field as

$$P_{\parallel} = mc^2 \int_{l_{\mathrm{min}}}^{l_{\mathrm{max}}} \frac{f}{1 + 1/q_f} \left(\frac{l}{l_{\mathrm{min}}}\right)^{C_0} \gamma_{\mathrm{inj}}\, \beta_R\, dl, \tag{7}$$

where l_{min} refers to the minimum current sheet size, l_{max} corresponds to largest scale current sheets, and $\gamma_{\mathrm{inj}} \propto \sigma$ (Comisso & Sironi 2019) is the mean particle Lorentz factor reached after being injected by the current sheet.

PIC simulations have consistently demonstrated the two-stage nature of particle acceleration in magnetized turbulence (Comisso & Sironi 2018, 2019, 2021; Nättilä & Beloborodov 2021) and any successful theory of particle acceleration must encompass not only stochastic acceleration effects but also account for initial acceleration by nonideal fields. Comisso & Sironi (2018, 2019) showed via particle tracking that the highest-energy particles usually first go through an injection phase that is associated with current sheets. If this is the case, then an acceleration theory for the injection phase requires both an understanding of how particles interacting with current sheets (or other dissipative structures) gain energy and how the distribution of dissipative regions depends on the initial plasma parameters. This work has focused on the latter, but a full acceleration theory will need to couple this with an adequate understanding of dissipation inside these structures. In Lemoine (2021), the author reviews a random walk through intermittent structures as informed by the large deviation theory. In the random walk with a time step t_{rw}, a particle is assumed to have a probability f_+ of gaining a momentum fraction g, a probability f_- of losing momentum fraction g, and a probability $1 - f_+ - f_-$ of not interacting in that time step. This model showed it was capable of reproducing a hardened particle spectrum, but applying it here requires an understanding of how g depends on σ and $\delta B_0/B_0$. Further still, to use this model as an acceleration theory would require the assumption that the particle dynamics inside of magnetized turbulence can be reduced to a Levy flight.

In this work, we combined intermittency analysis with phenomenological scaling theories to gain insights into the distribution of dissipative coherent structures within relativistic turbulent plasmas. Specifically, through the construction of SFs up to order 10 from 3D relativistic turbulent PIC simulations, we accurately measured the SF exponents ζ_p, which, when

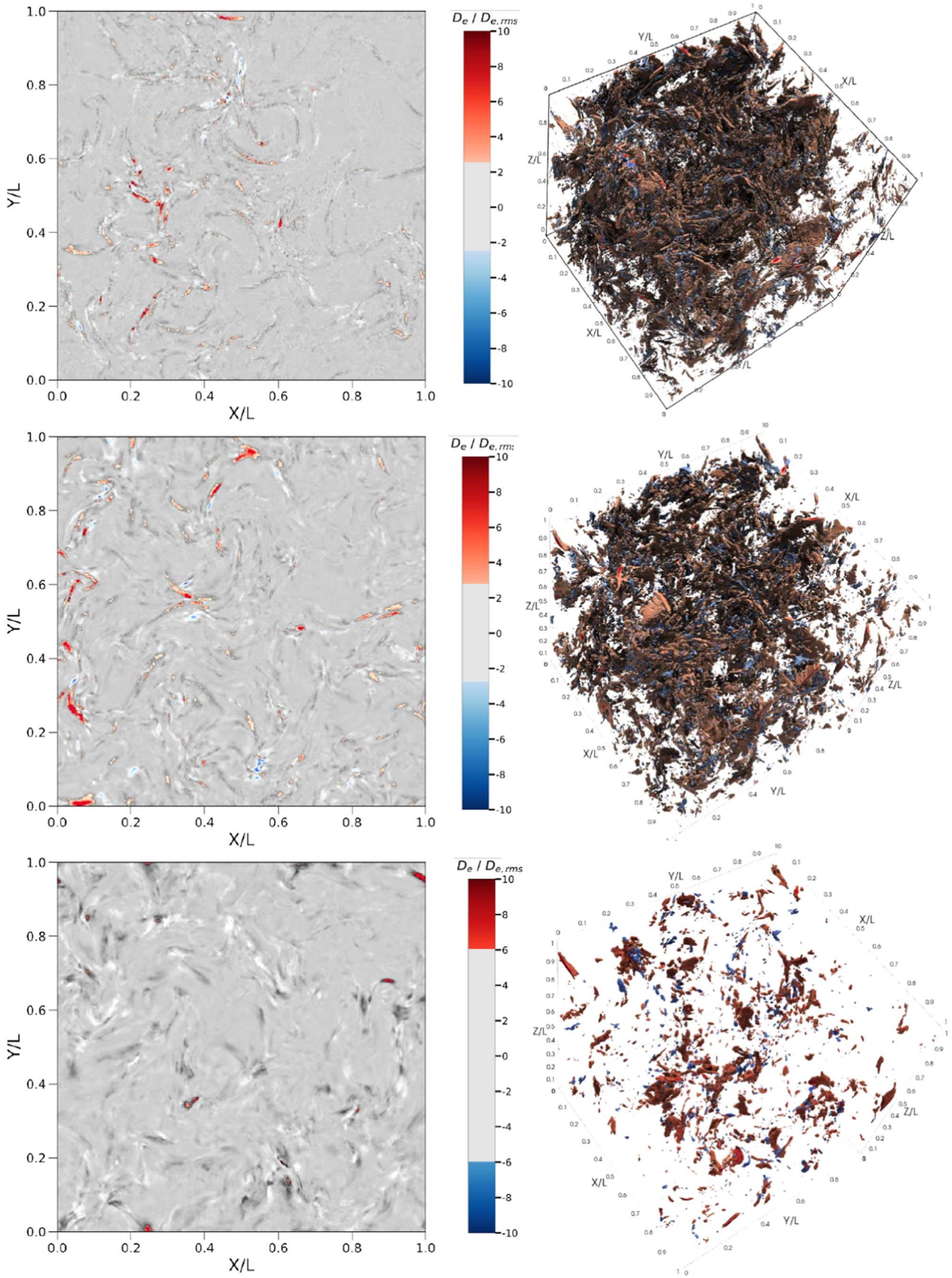

Figure 6. 2D representation (left) and 3D representation (right) illustrating the most dissipative structures. From top to bottom, these structures correspond to turbulence with $\sigma = 2.5$, 10, and 40. The figures show that as σ increases, the coherent structures become increasingly dissipative while becoming less volume filling.

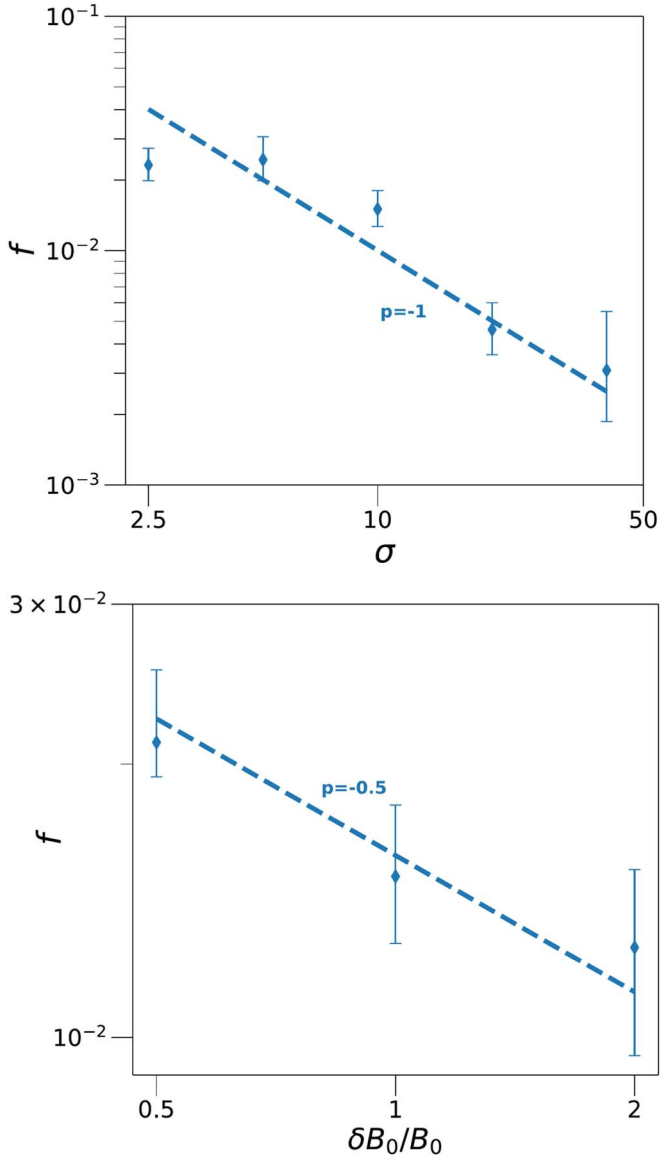

Figure 7. Top: dependency of the filling fraction f of the dissipative structures on the magnetization σ. Bottom: f dependence on $\delta B_0/B_0$. Dashed lines show a power law with a similar slope to data.

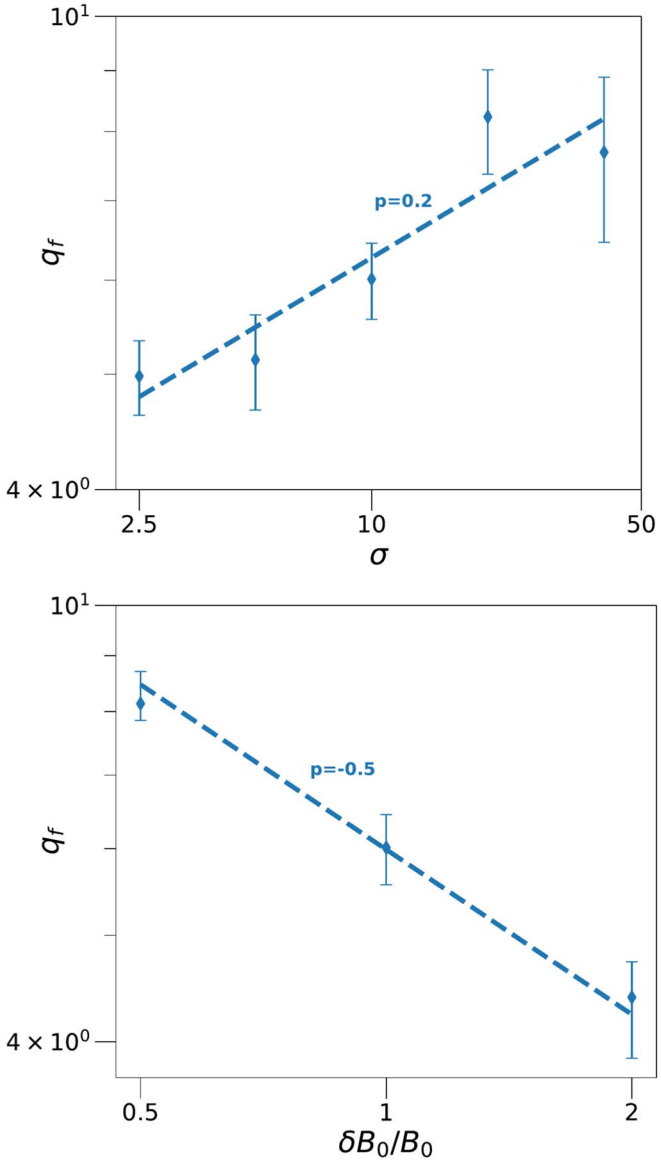

Figure 8. Top: dependence of $q_f = f_+/f_-$ on σ. Bottom: q_f dependence on $\delta B_0/B_0$. Dashed lines show a power law with a similar slope to data.

fitted to a generalized She–Leveque model, revealed the value of the codimension C_0 of the most dissipative structures. We then determined the 3D representation of these structures by identifying regions of significant dissipation that shared the same value of C_0. Once identified, we were able to determine the filling fraction and the subset of positive to negative work structures. All of this was done for a range of σ and $\delta B_0/B_0$ values, providing insights into how these properties scale within the regime of *relativistic turbulence*. The value of the codimension C_0 for the magnetic field generally increases for both σ and $\delta B_0/B_0$ going from 1, a value representative of a sheet, toward a value of 2, more filamentary-like. Nonetheless, when pinpointing the most dissipative structures with larger values of C_0, they exhibit characteristics more akin to discrete flux ropes rather than extended sheets. This suggests the possibility of current sheets becoming more tearing unstable, allowing the cascade to continue into smaller structures. Furthermore, we found that the filling fraction f of the dissipative structures decreases with σ and $\delta B_0/B_0$, plateauing at large values of σ. Additionally, the ratio of positive to negative work structures, q_f, increases with σ, leveling off at large σ values, while decreasing with $\delta B_0/B_0$. These results contribute to understanding the link between scaling theories and intermittent coherent structures, paving the way for the development of a physically informed turbulent acceleration theory.

Acknowledgments

Z.D. and D.G. acknowledge support from the NSF AST-2107802, AST-2107806, and AST-2308090 grants. L.C. acknowledges support from the NASA ATP award 80NSSC22K0667. We acknowledge computing resources provided by the Innovative and Novel Computational Impact on Theory and Experiment (INCITE) program, using resources of the Argonne Leadership Computing Facility, which is a DOE Office of Science User Facility supported under contract DE-AC02-06CH11357.

ORCID iDs

Zachary Davis https://orcid.org/0000-0002-0959-9991
Luca Comisso https://orcid.org/0000-0001-8822-8031
Dimitrios Giannios https://orcid.org/0000-0003-1503-2446

References

Band, D., Matteson, J., Ford, L., et al. 1993, ApJ, 413, 281
Bernstein, I. B., & Engelmann, F. 1966, PhFl, 9, 937
Birdsall, C. K., & Langdon, B. 1985, Plasma Physics via Computer Simulation (New York: McGraw-Hill)
Biskamp, D., & Müller, W.-C. 2000, PhPl, 7, 4889
Böttcher, M., & Dermer, C. D. 2010, ApJ, 711, 445
Buneman, O. 1993, Computer Space Plasma Physics (Tokyo: Terra Scientific), 67
Bykov, A. M., & Meszaros, P. 1996, ApJL, 461, L37
Comisso, L., & Jiang, B. 2023, ApJ, 959, 137
Comisso, L., & Sironi, L. 2018, PhRvL, 121, 255101
Comisso, L., & Sironi, L. 2019, ApJ, 886, 122
Comisso, L., & Sironi, L. 2021, PhRvL, 127, 255102
Comisso, L., Sobacchi, E., & Sironi, L. 2020, ApJL, 895, L40
Davis, Z., Rueda-Becerril, J. M., & Giannios, D. 2022, MNRAS, 513, 5766
Demidem, C., Lemoine, M., & Casse, F. 2020, PhRvD, 102, 023003
Dong, C., Wang, L., Huang, Y.-M., et al. 2022, SciA, 8, eabn7627
Dubrulle, B. 1994, PhRvL, 73, 959
Fermi, E. 1949, PhRv, 75, 1169
Ghisellini, G., Celotti, A., Fossati, G., Maraschi, L., & Comastri, A. 1998, MNRAS, 301, 451
Giannios, D. 2013, MNRAS, 431, 355
Goldreich, P., & Sridhar, S. 1995, ApJ, 438, 763
Iroshnikov, P. S. 1963, AZh, 40, 742
Kolmogorov, A. 1941, DoSSR, 30, 301
Kraichnan, R. H. 1965, PhFl, 8, 1385
Lazarian, A., Vlahos, L., Kowal, G., et al. 2012, SSRv, 173, 557
Lemoine, M. 2021, PhRvD, 104, 063020
Marscher, A. P. 2014, ApJ, 780, 87
Matthews, J. H., Bell, A. R., & Blundell, K. M. 2020, NewAR, 89, 101543
Miller, J. A., Larosa, T. N., & Moore, R. L. 1996, ApJ, 461, 445
Müller, W.-C., & Biskamp, D. 2000, PhRvL, 84, 475
Müller, W.-C., Biskamp, D., & Grappin, R. 2003, PhRvE, 67, 066302
Nättilä, J., & Beloborodov, A. M. 2021, ApJ, 921, 87
Politano, H., & Pouquet, A. 1995, PhRvE, 52, 636
She, Z.-S., & Leveque, E. 1994, PhRvL, 72, 336
Spitkovsky, A. 2005, in AIP Conf. Ser. 801, Astrophysical Sources of High Energy Particles and Radiation, ed. T. Bulik, B. Rudak, & G. Madejski (Melville, NY: AIP), 345
Wan, M., Matthaeus, W. H., Roytershteyn, V., et al. 2016, PhPl, 23, 042307
Zenitani, S., Hesse, M., Klimas, A., & Kuznetsova, M. 2011, PhRvL, 106, 195003
Zhang, H., Marscher, A. P., Guo, F., et al. 2023, ApJ, 949, 71
Zhdankin, V., Uzdensky, D. A., Werner, G. R., & Begelman, M. C. 2020, MNRAS, 493, 603
Zrake, J., & MacFadyen, A. I. 2012, ApJ, 744, 32
Zrake, J., & MacFadyen, A. I. 2013, ApJL, 763, L12